Macrophage network dynamics depend on haptokinesis for optimal local surveillance

Neil Paterson and Tim Lämmermann

Supplemental Information

Supplemental Figures S1–S6

Supplemental Table

Legends to Supplemental Videos S1–S9

Supplemental Figures

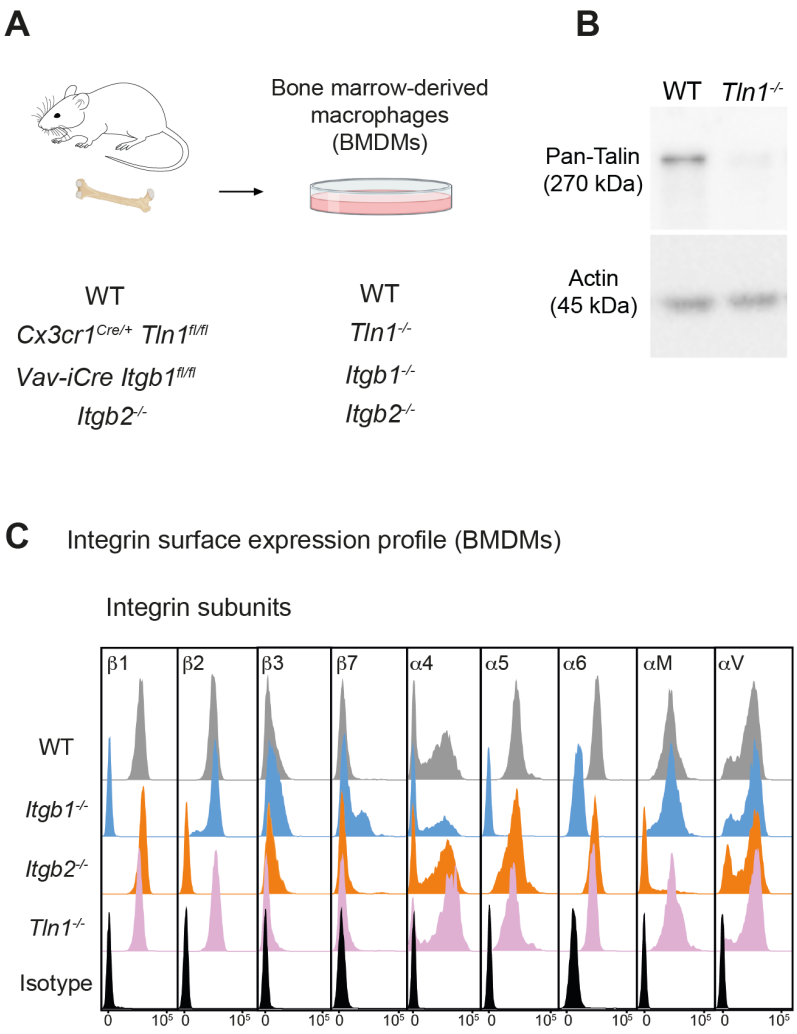

Figure S1. Characterization of mouse bone marrow-derived macrophages with impaired integrin functionality. (A) Scheme for the generation of bone marrow-derived macrophages (BMDMs) from conditional and constitutive knockout mouse models to obtain BMDMs depleted for talin-1 (*Tln1*$^{-/-}$) or cell surface integrins from the β1 family (*Itgb1*$^{-/-}$) or β2 family (*Itgb2*$^{-/-}$). **(B)** The efficiency of conditional talin-1 knockout was confirmed by immunoblot analysis (by using a pan-talin antibody (recognizing talin-1 and talin-2). Cell lysates were generated from WT and *Tln1*$^{-/-}$ BMDMs. Actin was used as loading control. **(C)** Flow cytometry analysis of integrin subunits expressed on the surface of WT, *Itgb1*$^{-/-}$, *Itgb2*$^{-/-}$ and *Tln1*$^{-/-}$ BMDMs. β1 integrin depletion leads to loss of fibronectin-binding α5β1 and laminin-binding α6β1 integrins from the cell surface of *Itgb1*$^{-/-}$ macrophages. A pool of the α4 subunit remains retained on the cell surface in combination with an upregulation of the corresponding β7 subunit. This switch from α4β1 to α4β7 heterodimers is a well-documented phenomenon for *Itgb1*$^{-/-}$ leukocytes. β2 integrin deficiency leads to loss of the αM subunit (CD11b) and thus αMβ2 (Mac-1, CR3) from the macrophage surface. Talin depletion in BMDMs leaves the cell surface integrin expression profile unchanged, and only interferes with the high-affinity state of integrins.

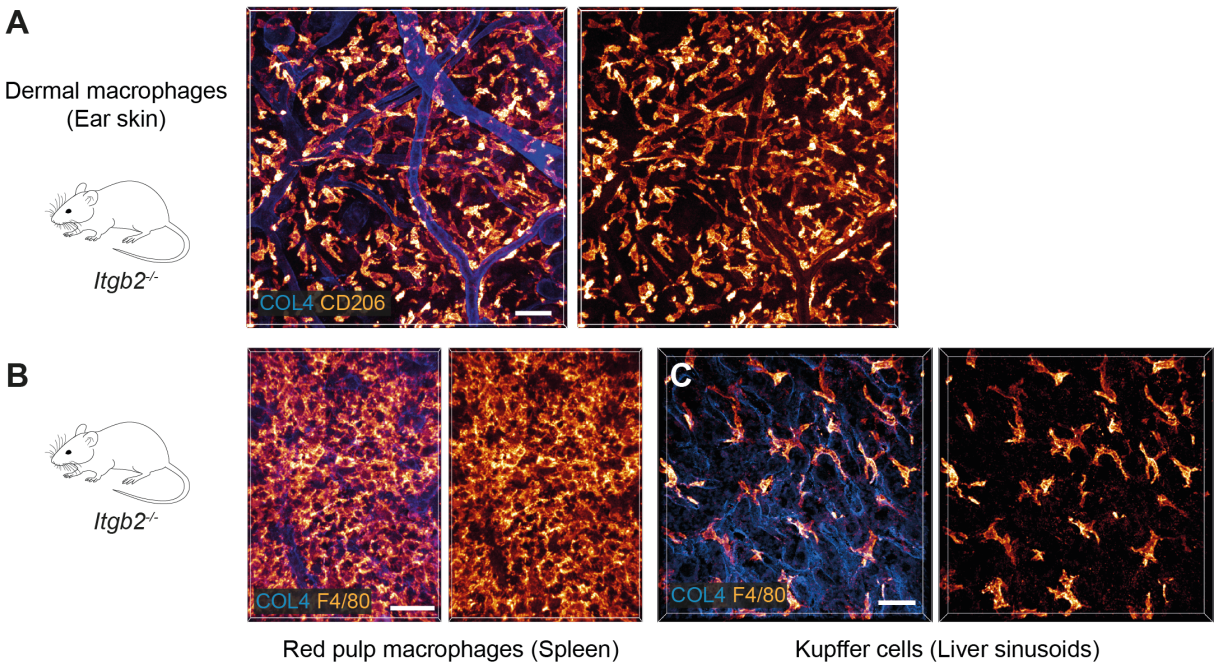

Figure S2. β2 integrins do not contribute to the mesenchymal shape of macrophages in mouse tissues. (A–C) Immunofluorescence analysis of ear skin dermis (A), spleen (B) and liver (C) tissues of adult *Itgb2*$^{-/-}$ mice. Endogenous macrophage subsets were detected with immuno-stainings against CD206 (A) and F4/80 (B,C) and fluorescence signal intensities displayed as glow heatmap color. Collagen IV (COL4)-expressing basement membrane (A, C) or reticular network (B) structures are also displayed (blue). All images are projections of several confocal *z*-planes. Scale bars: 50 µm (A), 30 µm (B, C).

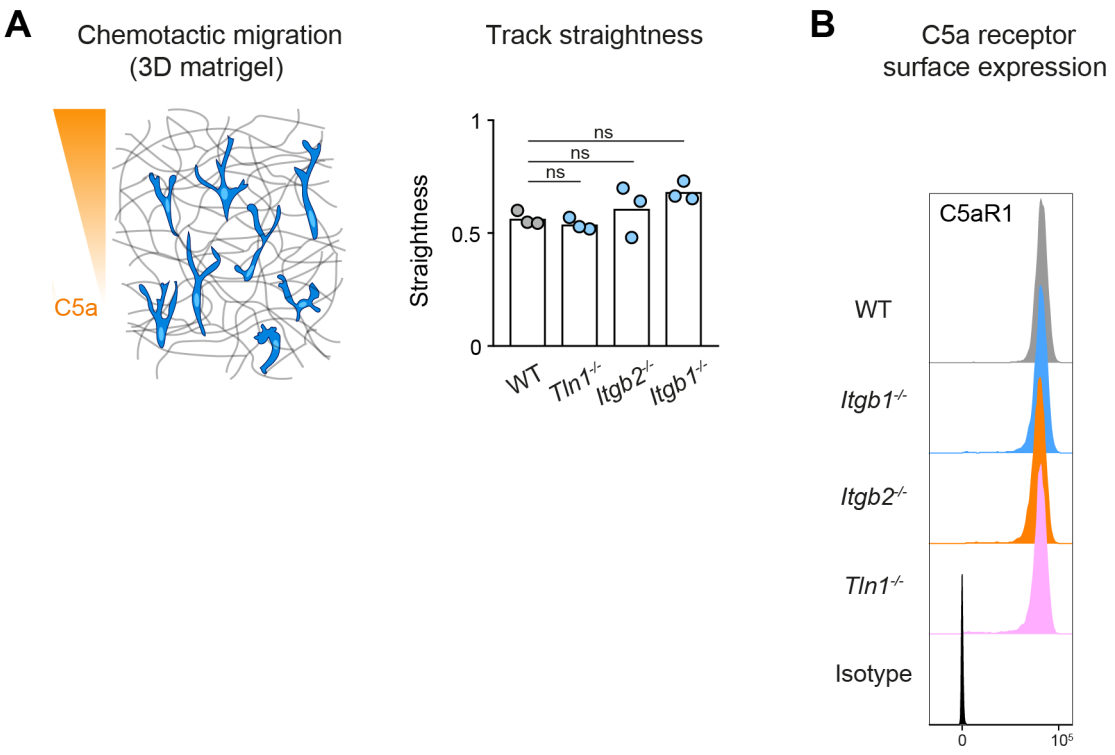

Figure S3. Track straightness and C5aR1 expression are unaltered in chemotaxing BMDMs with impaired integrin functionality. (A) Analysis of track straightness during BMDM chemotactic migration toward C5a gradients. Mean speed values were calculated from three biological replicates (*n*=3). In each biological replicate *N*=25 cells were tracked and analyzed. Bars in graph display the mean; ns: non-significant, Dunnett's multiple comparison (posthoc ANOVA). **(B)** Flow cytometry analysis of C5aR1 cell surface expression on WT, *Itgb1*$^{-/-}$, *Itgb2*$^{-/-}$ and *Tln1*$^{-/-}$ BMDMs. C5aR1 acts as the major chemotactic receptor for the chemoattractant C5a.

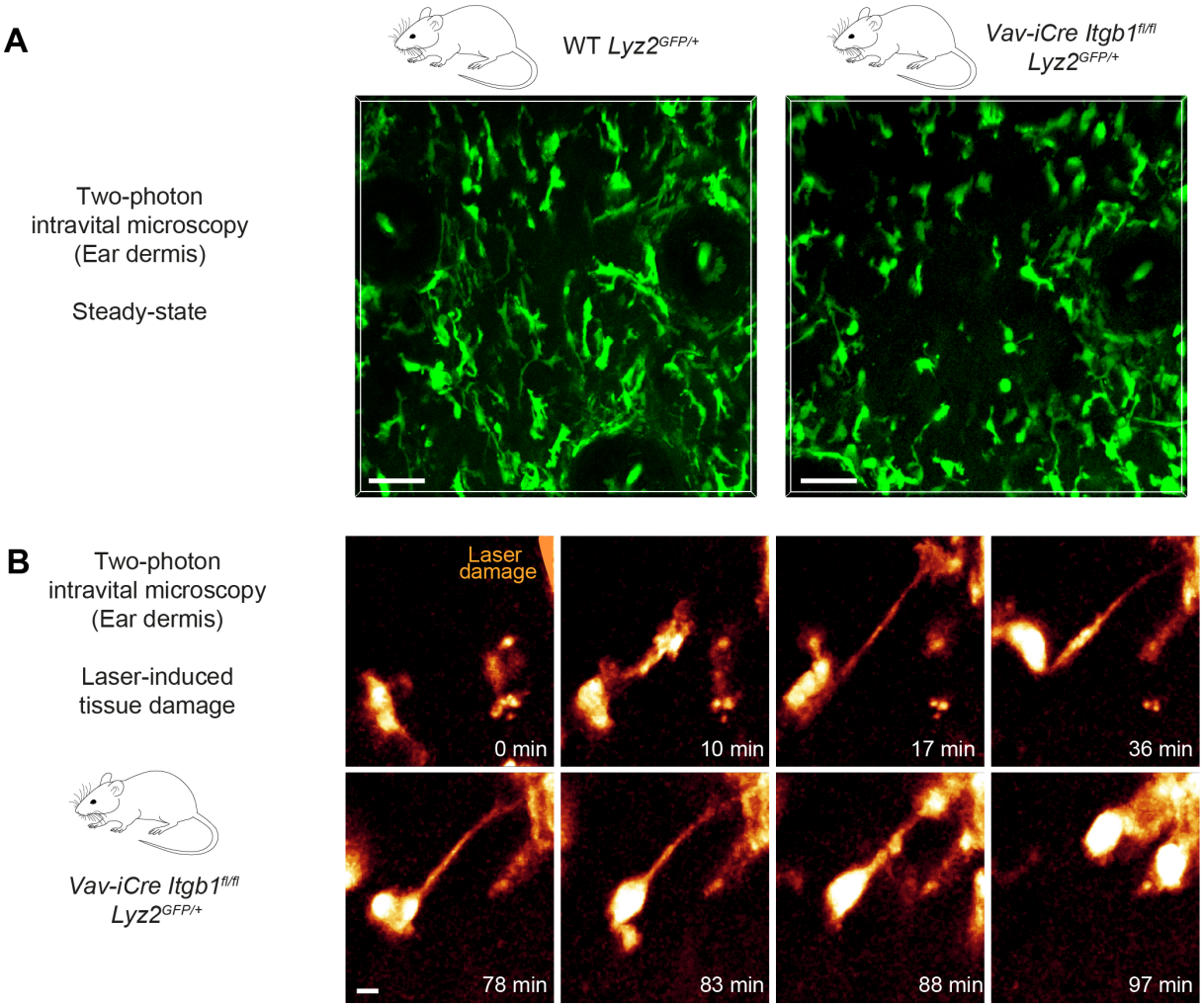

Figure S4. *Itgb1*-deficient macrophages perform chemotactic migration in mouse tissue. **(A)** Two-photon intravital microscopy of the dermal compartment in unchallenged ear skin reveals mesenchymal shapes with multiple elongated protrusions in GFP-positive macrophages of WT *Lyz2*$^{GFP/+}$ mice. In contrast, the majority of GFP-positive macrophages in the dermis of *Vav-iCre Itgb1*$^{fl/fl}$ *Lyz2*$^{GFP/+}$ mice showed more amoeboid-like morphologies and less pronounced cell protrusions. Scale bars: 50 µm. **(B)** Close-up view and time sequence of an *Itgb1*-deficient macrophage that chemotactically responds to a laser-induced tissue lesion. Despite lack of β1 integrins and loss of mesenchymal cell shape, these cells form directed protrusions and displace their cell bodies toward the wound site. Scale bar: 5 µm.

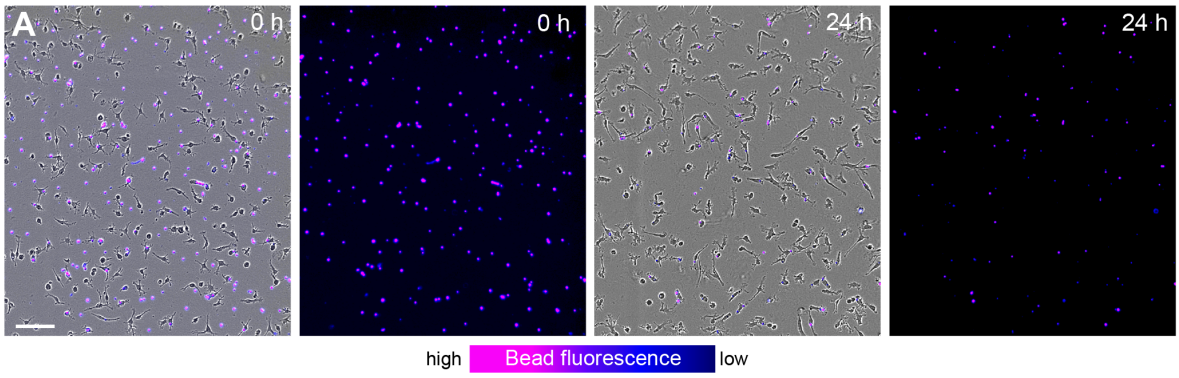
A
0 h
0 h
24 h
24 h
high
Bead fluorescence
low

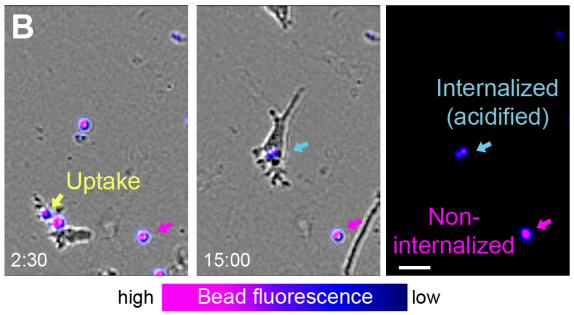
B
Uptake
2:30
15:00
Internalized
(acidified)
Non-
internalized
high
Bead fluorescence
low

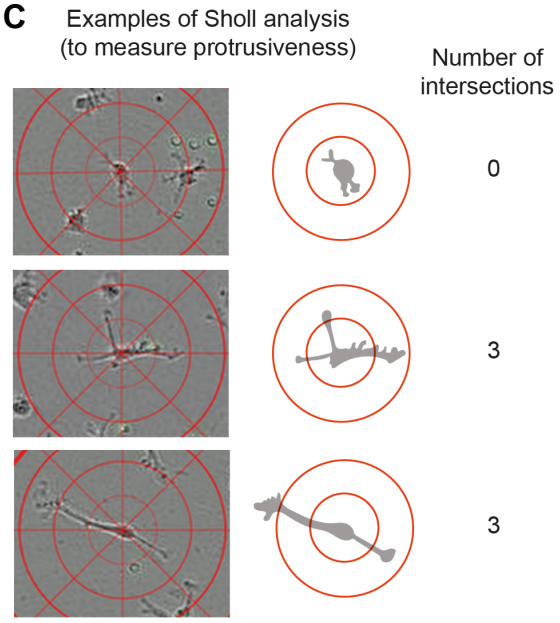
C
Examples of Sholl analysis
(to measure protrusiveness)
Number of
intersections
0
3
3

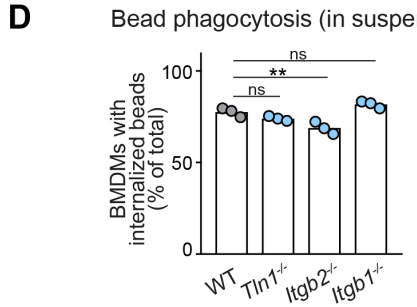
D
Bead phagocytosis (in suspension)
BMDMs with
internalized beads
(% of total)
100
50
0
ns
**
ns
WT
Tln1-/-
Itgb2-/-
Itgb1-/-

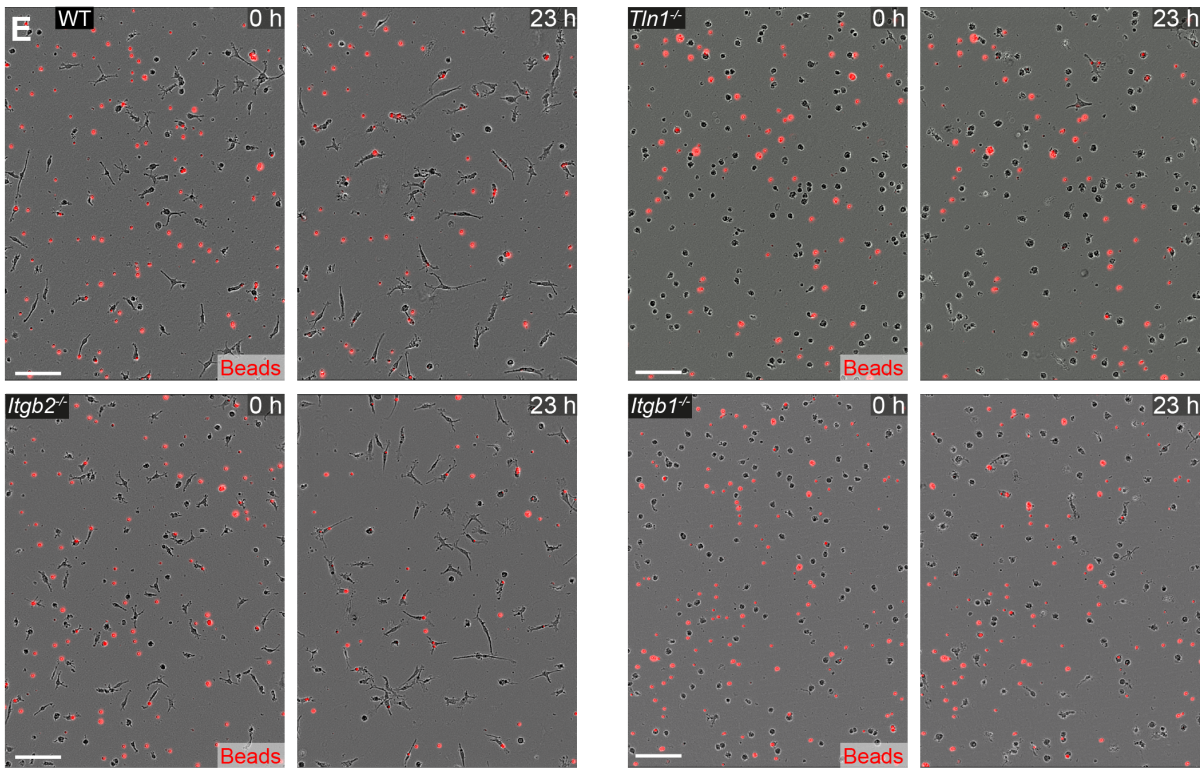
E
WT
0 h
23 h
Beads
Tln1-/-
0 h
23 h
Beads
Itgb2-/-
0 h
23 h
Beads
Itgb1-/-
0 h
23 h
Beads

Figure S5. Macrophages require β1 integrins for bead removal in matrigel, but not for bead phagocytosis in suspension. (A) Live cell imaging snapshots showing the start (0 h) and endpoint (24 h) of bead removal by a population of WT BMDMs (unstained). Fluorescent phosphatidylserine-attached beads were extracellular (red, 0 h) and fluorescence signal displayed as purple-blue heatmap color. At the onset of the experiment, most beads were extracellular and showed high fluorescence signal. After 24 h, the majority of beads was internalized by macrophages and showed low fluorescence signal. Scale bars: 100 µm. **(B)** Live cell imaging and close-up view of an individual WT BMDM that takes up a fluorescent bead at 2 h 30 min (yellow arrow). Approximately 12 hours later this internalized bead (light blue arrow) showed reduced signal due to fluorescence quenching in the acidic phagolysosomal compartment of the macrophage. In contrast, non-internalized beads (purple arrow) maintain the fluorescence signal over time. Scale bar: 20 µm**. (C)** Measurement of cell protrusiveness by Sholl analysis. The center points of individual macrophages are overlaid with layers of concentric rings (Sholl cells) at 25 µm intervals. The number of occasions Sholl shells are intersected by cellular process gives a measure of branch-based and elongation-based protrusiveness for an individual cell at a given timepoint. **(D)** Analysis of bead phagocytosis in cell suspensions. WT, *Itgb1*$^{-/-}$, *Itgb2*$^{-/-}$ and *Tln1*$^{-/-}$ BMDMs were kept in stirred cell suspensions with fluorescent beads for a 2 h incubation time. Bead internalization by macrophages was quantified by flow cytometry analysis, using a combination of intrinsic bead fluorescence and an annexin V labelling of extracellular beads. Representative experiment with N=3 technical replicates. Bars display the mean; ns: non-significant, $^{**}P \leq 0.01$, Dunnett's multiple comparison (posthoc ANOVA). **(E)** Live cell imaging snapshots showing the start (0 h) and a late timepoint (23 h) of bead removal by populations of WT, *Itgb1*$^{-/-}$, *Itgb2*$^{-/-}$ and *Tln1*$^{-/-}$ BMDMs. Extracellular, non-internalized fluorescent beads appear as bright red signal. Scale bars: 100 µm.

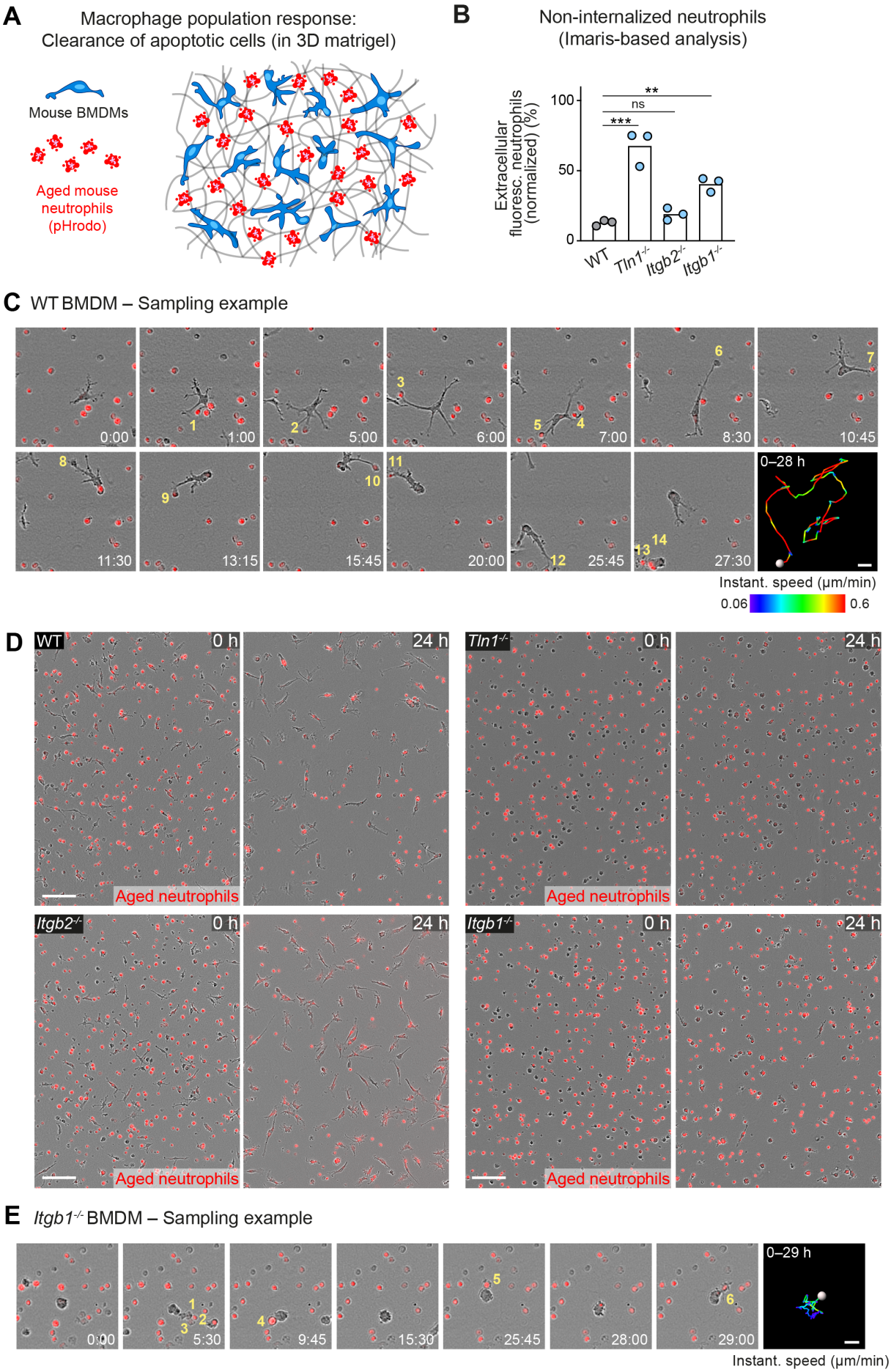
A
Macrophage population response:
Clearance of apoptotic cells (in 3D matrigel)
Mouse BMDMs
Aged mouse neutrophils (pHrodo)
B
Non-internalized neutrophils
(Imaris-based analysis)
Extracellular fluoresc. neutrophils (normalized) (%)
100
50
0
**
ns
***
WT
Tln1-/-
Itgb2-/-
Itgb1-/-
C WT BMDM – Sampling example
0:00
1:00
5:00
6:00
7:00
8:30
10:45
11:30
13:15
15:45
20:00
25:45
27:30
0–28 h
Instant. speed (µm/min)
0.06
0.6
D
WT
0 h
24 h
Aged neutrophils
Tln1-/-
Itgb2-/-
Itgb1-/-
E Itgb1-/- BMDM – Sampling example
0:00
5:30
9:45
15:30
25:45
28:00
29:00
0–29 h
Instant. speed (µm/min)
0.06
0.6

Figure S6. Haptokinetic sampling of dead cells optimizes efferocytosis in macrophage networks. (A) Scheme for studying the efferocytic response of macrophage networks in 3D *in vitro* matrices (same as in Figure 6A). **(B)** Analysis of dead neutrophil removal after 24 h by BMDM networks upon genetic interference with integrin functionality. Validation of our analysis based on the integrated software of the Incucyte live cell imaging system (see Figure 6D). Imaris software-based analysis determined only the fluorescence signals of extracellular, non-internalized neutrophils 24 h after start of the experiment. Neutrophil uptake is measured as an object count and displayed as normalized values of the initial neutrophil numbers (0 h) for three independent experiments (*N*=2–5 technical replicates, which means imaging wells with BMDMs and matrigel). Bars are mean; ***$P \leq 0.001$, **$P \leq 0.01$, ns: non-significant; Dunnett's multiple comparison (posthoc ANOVA). **(C)** Live cell imaging and close-up view of an individual WT BMDM that samples and ingests several pHrodo Red-labeled dead neutrophils over 28 h. Yellow numbers indicate individual engulfed cell corpses. The cell track over 28 h is pseudo-colored for instantaneous speed values. Scale bar: 20 µm. **(D)** Live cell imaging snapshots showing the start (0 h) and endpoint (24 h) of dead neutrophil (red) removal by populations of WT, *Itgb1*$^{-/-}$, *Itgb2*$^{-/-}$ and *Tln1*$^{-/-}$ BMDMs. Non-internalized dead neutrophils show bright red signal. Scale bars: 100 µm. **(E)** Live cell imaging and close-up view of an individual *Itgb1*$^{-/-}$ BMDM that samples and ingests several pHrodo Red-labeled dead neutrophils over 29 h. Yellow numbers indicate individual engulfed cell corpses. The cell track over 29 h is pseudo-colored for instantaneous speed values. Scale bar: 20 µm.

Supplemental Table

Figure	Statist. test		Posthoc test	
1D	**Kruskal-Wallis**	H=61.4, n(group)=3, P≤0.0001 N(Ctrl:CytoD)=25,25, N(Ctrl:Y27)=25,25	**Dunn's** Control:CytoD Control:Y27	 *** (P≤0.001) *** (P≤0.001)
1E	**ANOVA**	F(2, 6)=172.0, P≤0.0001	**Dunnett's** Control:CytoD Control:Y27	 *** (P≤ 0.001) *** (P≤0.001)
1G	**Kruskal-Wallis**	H=70.62, n(group)=4, P≤0.0001 N(WT: $Tln1^{-/-}$)=25,25, N(WT: $Itgb2^{-/-}$)=25,25, N(WT: $Itgb1^{-/-}$)=25,25	**Dunn's** WT: $Tln1^{-/-}$ WT: $Itgb2^{-/-}$ WT: $Itgb1^{-/-}$	 *** (P≤0.001) ns (P>0.05) *** (P≤0.001)
1H	**ANOVA**	F(3,8)=58.43, P≤0.0001	**Dunnett's** WT: $Tln1^{-/-}$ WT: $Itgb2^{-/-}$ WT: $Itgb1^{-/-}$	 *** (P≤0.001) ns (P>0.05) *** (P≤0.001)
3D	**Kruskal-Wallis**	H=62.26, n(group)=3, P≤0.0001 N(Ctrl:CytoD)=25,25, N(Ctrl:Y27)=25,25	**Dunn's** Control:CytoD Control:Y27	 *** (P≤0.001) *** (P≤0.001)
3E	**ANOVA**	F(2,6)=848.8, P≤0.0001	**Dunnett's** Control:CytoD Control:Y27	 *** (P≤0.001) *** (P≤0.001)
3F	**ANOVA**	F(3,96)=1.025, P=0.3851 N(WT: $Tln1^{-/-}$)=25,25, N(WT: $Itgb2^{-/-}$)=25,25, N(WT: $Itgb1^{-/-}$)=25,25	**Dunnett's** WT: $Tln1^{-/-}$ WT: $Itgb2^{-/-}$ WT: $Itgb1^{-/-}$	 ns (P>0.05) ns (P>0.05) ns (P>0.05)
3G	**ANOVA**	F(3,8)=0.5293, P=0.6746	**Dunnett's** WT: $Tln1^{-/-}$ WT: $Itgb2^{-/-}$ WT: $Itgb1^{-/-}$	 ns (P>0.05) ns (P>0.05) ns (P>0.05)
S3A	**ANOVA**	F(3,8)=2.926, P=0.0998	**Dunnett's** WT: $Tln1^{-/-}$ WT: $Itgb2^{-/-}$ WT: $Itgb1^{-/-}$	 ns (P>0.05) ns (P>0.05) ns (P>0.05)
4D	**Mann Whitn. *U* test**	U=871, N(WT)=37, N($Itgb1^{-/-}$)=55, P=0.2455	-	ns (P>0.05)
5E	**ANOVA**	F(2,6)=418.8, P≤0.0001	**Dunnett's** Control:CytoD Control:Y27	 *** (P≤0.001) ns (P>0.05)
5L	**ANOVA**	F(3,8)=37.13, P≤0.0001	**Dunnett's** WT: $Tln1^{-/-}$ WT: $Itgb2^{-/-}$ WT: $Itgb1^{-/-}$	 *** (P≤0.001) ns (P>0.05) *** (P≤0.001)
5O	**ANOVA**	F(3,8)=33.30, P≤0.0001	**Dunnett's** WT: $Itgb1^{-/-}$ (2x)	 ns (P>0.05)
S5D	**ANOVA**	F(3,8)=15.81, P≤0.001	**Dunnett's** WT: $Tln1^{-/-}$ WT: $Itgb2^{-/-}$ WT: $Itgb1^{-/-}$	 ns (P>0.05) ** (P≤0.01) ns (P>0.05)

6D	**ANOVA**	F(3,8)=33.94, P≤0.0001	**Dunnett's** WT: Tln1$^{-/-}$ WT: Itgb2$^{-/-}$ WT: Itgb1$^{-/-}$	 ***(P≤0.001) ns (P>0.05) ** (P≤0.01)
S6B	**ANOVA**	F(3,8)=35.7, P≤0.0001	**Dunnett's** WT: Tln1$^{-/-}$ WT: Itgb2$^{-/-}$ WT: Itgb1$^{-/-}$	 ***(P≤0.001) ns (P>0.05) ** (P≤0.01)
7D	**unpaired two-tailed *t* test**	t=4.695, df=4, P=0.0093	-	** (P≤0.01)

Legends to Supplemental Videos S1 to S9

Video S1: Random motility of macrophages in 3D matrices (related to Figure 1)
Bone marrow derived macrophages (BMDMs) were cultivated from WT mice and embedded in matrigel. Live cell migration and shape changes were recorded over 20 h with phase-contrast microscopy using an Incucyte S3 instrument. This video relates to Figure 1B.

Video S2: Talin-1 and β1 integrins control the mesenchymal shape and random motility of macrophages in matrigel (related to Figure 1)
First part: Comparison of cell shape and migratory behavior of WT, *Tln1*$^{-/-}$, *Itgb2*$^{-/-}$ and *Itgb1*$^{-/-}$ BMDMs in matrigel. Live cell migration and shape changes were recorded over 20 h with phase-contrast microscopy using an Incucyte S3 instrument. Second part: Comparison of matrigel-embedded BMDMs from *Vav-iCre* $^{+/-}$ *Tln1*$^{fl/fl}$ *Lifeact-GFP*$^{+/-}$ and WT *Lifeact-GFP*$^{+/-}$ mice. Live cell shape changes and protrusion dynamics were recorded over 10 min with phase-contrast microscopy using confocal fluorescence microscopy. Lifeact-GFP signal is displayed as glow heatmap color. This video relates to Figures 1F–K.

Video S3: Integrin-independent chemotactic movement of macrophages in matrigel (related to Figure 3)
WT, *Tln1*$^{-/-}$, *Itgb2*$^{-/-}$ and *Itgb1*$^{-/-}$ BMDMs were embedded in matrigel and exposed to a chemotactic C5a gradient. Chemotactic migration along the gradient was recorded over 20 h with phase-contrast microscopy using an Incucyte S3 instrument. The lower row shows an animation of chemotactic cell tracks over the same time period. This video relates to Figures 3C, F and G.

Video S4: Amoeboid-like macrophages still perform chemotactic responses in mouse tissue (related to Figure 4)
Two-photon intravital microscopy was performed on the ear skin of *Vav-iCre Itgb1*$^{fl/fl}$ *Lyz2*$^{GFP/+}$ and littermate control mice, which had received neutrophil-depleting Anti-Ly6G antibody to avoid the presence of neutrophils in imaging field of views. Chemotactic protrusion formation and cell body displacement toward a laser-induced tissue injury (orange area) of GFP-expressing dermal macrophages in WT mice (first part) and conditional *Itgb1*-deficient mice (second part) were recorded over 90 min. GFP signal is displayed as glow heatmap color. This video relates to Figure 4.

Video S5: Movement and protrusiveness as two sampling strategies for bead removal by macrophage networks (related to Figure 5)

BMDMs were embedded in matrigel in the presence of fluorescent beads (red) coated with phosphatidylserine, an “eat-me” signal for macrophages. BMDMs were treated with vehicle or the ROCK inhibitor Y27632 and bead sampling activity recorded over 20 h with phase-contrast and fluorescence microscopy using an Incucyte S3 instrument. Control BMDMs are migratory and cover larger distance to sample beads (first part). Y27632-treated macrophages have reduced migration speed, but the increase in protrusiveness still allows efficient bead sampling (second part). This video relates to Figures 5C–H.

Video S6: Haptokinesis is required for optimal bead removal by macrophage networks (related to Figure 5)

β1 integrin-deficient BMDMs were embedded in matrigel in the presence of fluorescent beads (red) coated with phosphatidylserine, an “eat-me” signal for macrophages. Bead sampling activity was recorded over 19 h with phase-contrast and fluorescence microscopy using an Incucyte S3 instrument. Amoeboid-shaped *Itgb1*$^{-/-}$ BMDMs hardly move or form pronounced protrusions. Still, these macrophages are able to take up and ingest beads, but only beads in close vicinity to the cells. This video relates to Figures 5I–M.

Video S7: Efficient efferocytosis of aged neutrophils by macrophage networks (related to Figure 6)

WT BMDMs were embedded in matrigel in the presence of aged neutrophils that were labeled with pHrodo-Red (red). Fluorescent dead neutrophils were extracellular, before they were engulfed and removed by the macrophage network over time. Efficient efferocytosis in this assay relies on the interpretation of “find-me” and “eat-me” signals from dead neutrophils. The efferocytic activity of the macrophage network was recorded over 30 h with phase-contrast and fluorescence microscopy using an Incucyte S3 instrument. This video relates to Figures 6A and 6B.

Video S8: Examples of efferocytic WT macrophages (related to Figure 6)

WT BMDMs were embedded in matrigel in the presence of aged neutrophils that were labeled with pHrodo-Red (red). Three examples of macrophages that sequentially sample and ingest dead neutrophils are shown, revealing a phenotypic spectrum for efficient efferocytosis in WT cells. Cell 3 provides a good example of very directed protrusion formation toward dead neutrophil material. Efferocytic activity was recorded over 14, 28 and 18 h with phase-contrast and fluorescence microscopy using an Incucyte S3 instrument. This video relates to Figures 6E and S6C.

Video S9: Haptokinesis is required for optimal efferocytosis by macrophage networks (related to Figure 6)

WT and *Itgb1*$^{-/-}$ BMDMs were embedded in matrigel in the presence of aged neutrophils that were labeled with pHrodo-Red (red). WT BMDMs are migratory and cover larger distance to sample and engulf dead neutrophils. In contrast, *Itgb1*$^{-/-}$ BMDMs hardly move or form pronounced protrusions, allowing only uptake of dead neutrophils in close vicinity to them. Efferocytic activity was recorded over 23 h with phase-contrast and fluorescence microscopy using an Incucyte S3 instrument. This video relates to Figures 6E and 6F.